A comparative evaluation of a RARE-based single-shot pulse sequence for diffusion-weighted MRI of musculoskeletal soft-tissue tumors

Olaf Dietrich[1], José G. Raya[1], Julia Sommer[1], Michael Deimling[2], Maximilian F. Reiser[1], Andrea Baur-Melnyk[1]

[1]Department of Clinical Radiology – Großhadern, Ludwig Maximilian University of Munich, Germany
[2]Siemens Medical Solutions, Erlangen, Germany

ELECTRONIC PREPRINT VERSION:
Not for commercial sale or for any systematic external distribution by a third party
The original publication is available at <http://www.springerlink.com>.
Final version: *European Radiology* 2005; **15:** 772–783. <URL:http://dx.doi.org/10.1007/s00330-004-2619-3>

Abstract

The purpose of this study was to evaluate the feasibility of a centric-reordered modified RARE sequence (mRARE) for single-shot diffusion-weighted magnetic resonance imaging (DWI) of soft-tissue tumors in the musculoskeletal system. In evaluation of this sequence, DWI was performed in a liquid phantom, in excised human tumor samples embedded in bovine muscle, and in 9 patients suffering from different types of soft-tissue tumors. The measurements were compared to DWI using a spin-echo sequence and a single-shot EPI sequence. The phantom measurements in water and dimethyl sulfoxide showed a difference of less than 5 % comparing the ADCs determined by the mRARE sequence and the two other techniques. Comparing mRARE and EPI, the differences in the ADC were about 10 % in the excised tumor tissue and typically about 15 % in vivo. ADCs between 0.8 and 1.4×10^{-3} mm^2/s depending on the tumor type were found in solid tumor tissue; in cystic tumor areas, ADCs greater than 2.0×10^{-3} mm^2/s were determined with the mRARE and the EPI sequence. Diffusion-weighted images of the mRARE sequence were less distorted than those acquired with the single-shot EPI sequence and provided more anatomic information since muscle and fat signals were considerably higher.

Keywords:
Magnetic resonance (MR), diffusion study;
Magnetic resonance (MR), tissue characterization;
Neoplasms, MR;
Sarcoma

Corresponding author:
Olaf Dietrich, PhD
Ludwig Maximilian University of Munich
Department of Clinical Radiology – Großhadern
Marchioninistr. 15
81377 Munich
GERMANY
Telephone number: +49 (0)89 7095-3623
Fax number: +49 (0)89 7095-4627
E-mail: od@dtrx.net

Introduction

Diffusion-weighted magnetic resonance imaging (DWI) in vivo reflects the microscopic stochastic Brownian motion of water molecules in the tissue. In recent years, DWI has been established as valuable diagnostic tool. Two of its most important clinical applications are the early detection of ischemic lesions in the brain [1–3] and the tracking of white matter fibers using diffusion tensor imaging (DTI) [4–6]. Other clinical applications include characterization of multiple sclerosis lesions, abscesses, and tumors of the brain [7–10]. DWI has also been performed outside the brain, e.g. in the abdominal organs (liver, kidneys, ovaries) [11–14] and in various musculoskeletal structures such as muscle, synovial fluid, intervertebral discs, tumor tissue, and bone marrow [15–28]. Several of these studies indicate that DWI may be useful for the differentiation between benign and malignant lesions [11, 21, 23, 25, 26], between viable and necrotic tumor regions [29], or between tumor recurrences and post-therapeutic soft-tissue changes [19]. Diffusion coefficients of malignant tumors or tumor recurrences have been found to be significantly lower than those of benign masses, necrotic tumor tissue, or post-therapeutic changes, probably due to the more densely packed tumorous cells in malignant tumors that restrict the water diffusion [11, 19, 21, 23, 29]. These findings explain the motivation to further optimize DWI in the musculoskeletal system and thus to provide a technique that can contribute to the differentiation of malignant and benign tumors.

Several types of magnetic resonance (MR) pulse sequences can be modified for DWI by inserting additional diffusion-sensitizing gradients. In the presence of molecular motion, these gradients dephase the nuclear spins and thus attenuate the image intensity depending on the diffusion coefficient *D* [30]. Whereas diffusion-sensitized single-shot spin-echo echo planar imaging (EPI) sequences are now regarded as the standard approach for DWI and DTI of the brain, no such agreement exists with respect to DWI outside the brain. Several alternative techniques for DWI of musculoskeletal structures have been applied, including spin echo (SE) or stimulated echo sequences with navigator echo motion correction [17, 21], line scan imaging techniques [27], MR sequences with radial k-space acquisition [18], steady-state free precession (SSFP) sequences [23], segmented (i.e., multi-shot) EPI sequences [22], and single-shot sequences based on the acquisition of a series of spin echoes such as turbo spin echo (TSE) methods [25, 26]. This last group appears especially promising for robust DWI examinations in clinical routine because these sequences are less motion-sensitive due to the single-shot approach and at the same time the acquisition of multiple spin echoes is less sensitive to susceptibility artifacts than the EPI readout. Therefore, it can be expected that the two main limiting factors of DWI outside the brain, image quality and acquisition time, can be overcome using single-shot TSE sequences.

The purpose of this study was to evaluate the feasibility of a single-shot multi spin echo sequence for DWI of soft-tissue tumors in the musculoskeletal system by measuring apparent diffusion coefficients (ADCs) in a liquid phantom and in soft-tissue tumors in vitro and in vivo, by calculating the reproducibility of the determined ADCs, and by comparing the results to measurements with SE and EPI sequences.

Materials and methods

The diffusion-weighting single-shot multi spin echo sequence evaluated in this study is a centric-reordered RARE (rapid acquisition with relaxation enhancement) [31] version of the diffusion-weighting "displaced U-FLARE" sequence suggested by Norris et al. in 1992 [32, 33]. The sequence has been called "displaced" because only echoes of even parity are acquired by means of an additional gradient immediately before the readout gradient. This is done because the equal RF spacing of the conventional RARE sequence had to be abandoned in order to insert the diffusion-sensitizing gradients; hence, the Carr-Purcell-Meiboom-Gill (CPMG) condition is not longer fulfilled and echoes of even and odd parity may cancel each other. In this work, we use the term "modified RARE" (mRARE) to refer to this pulse sequence. When the minimum possible TE is chosen, the sequence starts with 4 dummy cycles to reduce intensity variations between consecutive echoes; increasing the TE increases the number of dummy cycles while the k-space sampling remains centric reordered. Diffusion weighting is achieved by two pairs of bipolar gradients with two 180° pulses following gradient lobe 1 and 3, similar to the scheme suggested by Reese et al. [34].

This diffusion-weighting mRARE sequence was evaluated in three steps: (1) in phantom measurements, (2) in measurements of excised tumor and muscle tissue in vitro, and (3) in patient measurements. In steps 1 and 2 we compared the sequence

with a diffusion-weighting SE sequence representing the standard method for diffusion measurements in vitro and with an EPI diffusion sequence as the standard method for measurements in vivo. Initial experiments with the SE sequence (without navigator motion correction) in vivo showed a very high level of motion artifacts resulting in images of non-diagnostic quality in most slices. Because of the high motion sensitivity and the long acquisition duration, the SE sequence was not applied in the patient measurements.

All measurements were performed on 1.5 T whole-body MR systems, either a Magnetom Sonata Maestro Class (Siemens, Erlangen, Germany) with high-performance gradients (maximum gradient amplitude 40 mT/m, maximum gradient slope 200 mT/m/ms) or a Magnetom Symphony Maestro Class (Siemens, Erlangen, Germany) with Quantum gradients (maximum gradient amplitude 30 mT/m, maximum gradient slope 100 mT/m/ms).

Phantom measurements

The phantom consisted of 4 glass cylinders (diameter 68 mm) with liquids of different diffusivities: water, acetone, polyethylene glycol (PEG), and dimethyl sulfoxide (DMSO). The phantom was measured in the Sonata scanner using two flexible phased-array surface coils positioned below and on top of the phantom. All diffusion measurements were performed at room temperature (24 °C) with diffusion weightings (b-values) of 50, 250, 500, and 750 s/mm^2 applied in read-out, phase-encoding, and slice direction. All images were acquired with a 128×96 matrix (read × phase) and a corresponding rectangular field of view (FOV) of 280×210 mm^2 in the coronal plane (isotropic in-plane resolution: 2.2×2.2 mm^2); the slice thickness was 5 mm and 3 slices were acquired in each acquisition. All other sequence parameters of the SE, EPI, and mRARE sequence are listed in Table 1. Averaging was performed on magnitude data for both single-shot sequences to avoid image artifacts due to motion-induced phase variations.

In order to evaluate the reproducibility of the measurements all data were acquired 4 times on two different days, thus enabling us to assess a combination of short-term and long-term stability of the measured diffusion parameters. Using linear regression analysis we calculated the ADCs in large circular regions of interest (ROIs) in all 4 test liquids together with the standard deviation of the ADC (describing how well the signal attenuation in each ROI agrees with the expected exponential decay for increasing diffusion weighting). These values were compared between the different pulse sequences. To assess the stability of the measurements, we calculated the standard deviation of the four repetitions and normalized it to the mean value of the ADC. We defined the reproducibility of a measurement to be the difference of this quotient to 1, i.e. 1 – (std. dev. / mean value). In the case of perfect reproducibility, i.e., identical ADCs in all repetitions, this definition gives a result of 100 %. The reproducibility is 0 if the standard deviation equals the mean value of the ADC, and, in theory, the reproducibility might become less than zero for very large standard deviations. Finally, the SNR of the sequences was determined in the water cylinder for all three diffusion directions and a b-value of 50 s/mm^2 by the difference image method suggested by Firbank et al. [35].

Measurements of excised tumor tissue and muscle

We embedded formalin-fixated excised tumor tissue of four different human soft-tissue tumors within thick slices of bovine muscle to provide an environment similar to the original tumor location. The tumors were histologically confirmed to be liposarcomas of grade1 (sample 1) and grade 3 (sample 3), a high-grade pleomorphic sarcoma (sample 2), and a carcinosarcoma (sample 4). Diffusion-weighted MRI was performed on these samples with the same pulse sequences as described for the phantom measurements in the previous section; however, only one diffusion direction (readout direction) was assessed using the spin-echo EPI sequence. The FOV of all sequences was adapted to the smaller sample size by setting it to 160×120 mm^2 (isotropic in-plane resolution: 1.25×1.25 mm^2). The samples were examined at the Sonata scanner in a dedicated wrist coil providing a good fill factor. ADCs and their standard deviations were calculated for ROIs positioned within the tumor samples and within homogeneous muscle tissue. The diffusion anisotropy was estimated from the measurements in three orthogonal directions by determining the ratio of the largest and the smallest ADC.

Patient measurements

9 patients with histologically confirmed soft-tissue tumors of the extremities (Table 4) were examined with diffusion-weighted imaging in addition to the standard clinical routine examination. All patients gave informed consent to participate in the study, which had local Ethics Committee approval.

The diffusion-weighted single-shot mRARE sequence and the single-shot spin-echo EPI sequence described above were applied in all patients with diffusion-weightings of 50, 250, 500, and 750 s/mm^2 in read-out direction. FOV and slice positioning as well as the receiver coil system were adapted to the different locations of the pathologies. Of the 9 patients, three (patients 1, 5, and 7) were examined on the Symphony scanner, the other six on the Sonata scanner. ADCs were determined as ADC maps and additionally measured in small homogeneous areas of viable tumor tissue showing strong contrast enhancement and, if present, in necrotic/cystic areas without contrast enhancement on T1-weighted SE images post Gd-DTPA application; if the SNR was sufficiently high, the ADC of muscle was calculated as well.

Results

Phantom measurements

The ADCs determined in the phantom are summarized in Table 2. Averaged over all three diffusion directions, the diffusion coefficient in water was 2.206×10^{-3} mm^2/s for the SE sequence, 2.294×10^{-3} mm^2/s for the mRARE sequence, and 2.243×10^{-3} mm^2/s for the EPI sequence. Thus, the diffusivity determined using the mRARE sequence differed by about 3.1 % from the average diffusion coefficient of the SE and EPI sequence. For acetone the difference between the mRARE sequence and the two other sequences was 15 %, for PEG 20 %, and for DMSO 5.4 %. The error of the linear regression varied between 0.2 % and 5 % for all measurements except for the determination of the diffusivity in acetone with errors up to 60 %.

The reproducibility varied between 92.6 % and 99.6 % for the measurements in water, PEG, and DMSO, and between 44.2 % and 98.2 % in acetone, as shown in Table 2. Averaging all measurements in water, PEG, and DMSO, the mean reproducibility was 97.9 % for the SE sequence, 96.6 % for the mRARE sequence, and 98.3 % for the EPI sequence.

The SNR of the water signal applying a b-value of 50 s/mm^2 is also given in Table 2. Averaging the signal-to-noise ratios over all 3 diffusion directions, we determined an SNR of 98 for the SE sequence, of 266 for the mRARE sequence, and of 137 for the EPI sequence.

Figure 1 shows image examples from all three sequences as well as quantitative ADC maps calculated from the diffusion-weighted images. There are no visible geometric distortions in the SE and mRARE images in contrast to the EPI sequence in which the DMSO and the water cylinders appear to overlap and the acetone cylinder is displaced in direction of the image border. Ghosting artifacts are visible in the mRARE and the EPI results, especially in the ADC maps. Although not visible in the images shown here, motion artifacts occurred in some of the spin echo images depending on the diffusion direction (image intensity propagated outside the phantom in phase-encoding direction).

The measurement time for 3 slices and 4 b-values was 384 s for the SE sequence (without averaging), 120 s for the mRARE sequence (10 averages), and 36 s for the EPI sequence (2 averages).

Table 1. Sequence parameters.

	SE	EPI	mRARE
TR (ms)	1000	3000	3000
TE (ms)	64	92	111
BW (Hz/pixel)	130	1345	260
Averages	1	2	10
Flip angle (refocusing)	180°	–	150°
Matrix	128×96 (read×phase)		
b-values (s/mm^2)	50, 250, 500, 750		

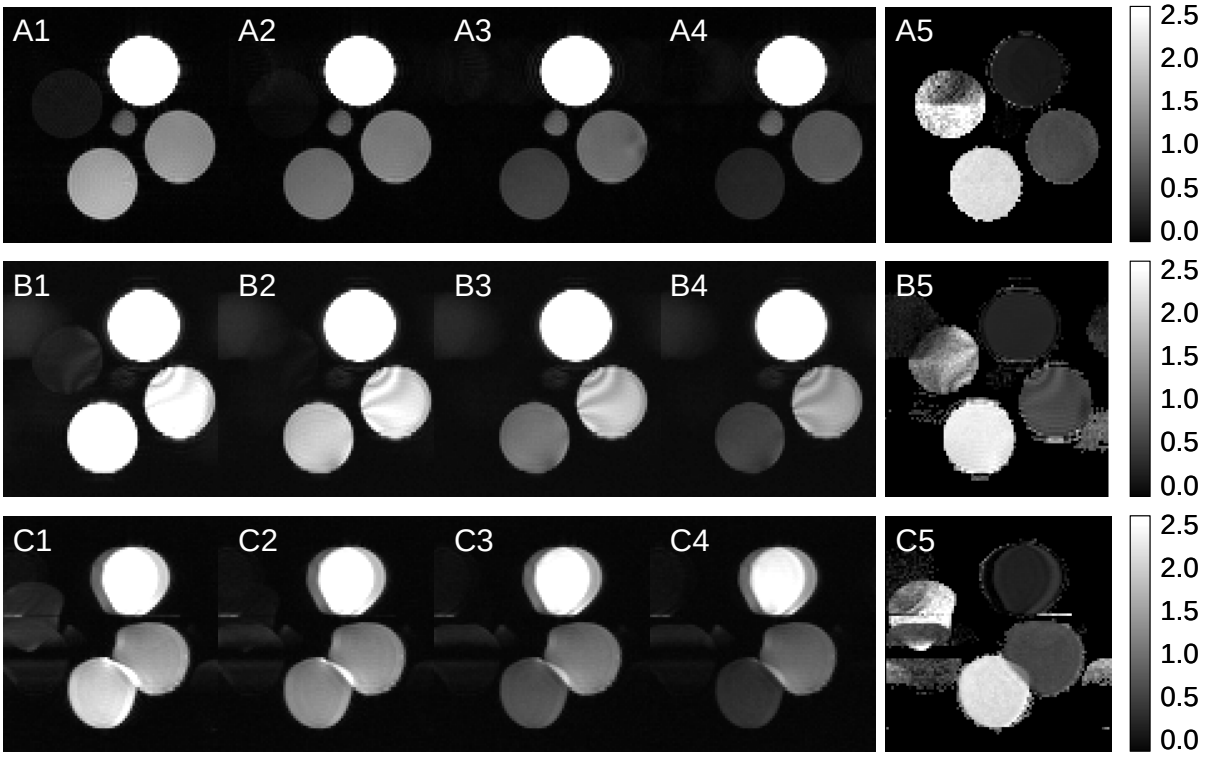

Figure 1. Image examples of phantom diffusion measurements. Row A: spin echo sequence, row B: single-shot multiple spin-echo sequence, row C: EPI sequence. Column 1…4: diffusion-weighted images with b-values 50, 250, 500, and 750 s/mm^2, column 5: ADC maps, scaled from 0 to 2.5×10^{-3} mm^2/s. The phantom contains four liquids: PEG (at the top) and (clock-wise) DMSO, water, and acetone. In the center of the phantom is a fat phantom that is visible only on the spin echo images.

Table 2. Comparison of diffusion measurements in test liquids.

	SE Read	SE Phase	SE Slice	mRARE Read	mRARE Phase	mRARE Slice	EPI Read	EPI Phase	EPI Slice
ADC[a] H_2O	2.218 (0.006)	2.146 (0.008)	2.255 (0.005)	2.360 (0.038)	2.238 (0.072)	2.285 (0.062)	2.227 (0.005)	2.216 (0.003)	2.285 (0.004)
ADC[a] Acetone	3.218 (0.456)	1.126 (0.656)	2.965 (0.530)	4.268 (0.333)	2.159 (0.747)	3.872 (0.367)	3.547 (0.348)	3.617 (0.365)	3.514 (0.385)
ADC[a] PEG	0.259 (0.007)	0.253 (0.008)	0.256 (0.005)	0.387 (0.011)	0.363 (0.013)	0.359 (0.009)	0.337 (0.002)	0.378 (0.004)	0.370 (0.005)
ADC[a] DMSO	0.738 (0.016)	0.727 (0.03)	0.717 (0.026)	0.738 (0.022)	0.643 (0.034)	0.709 (0.036)	0.719 (0.001)	0.720 (0.003)	0.798 (0.002)
Repr[b] H_2O	98.2 %	98.3 %	98.7 %	98.6 %	95.4 %	96.9 %	98.9 %	99.0 %	98.6 %
Repr[b] Acetone	91.4 %	44.2 %	78.9 %	78.2 %	69.5 %	81.2 %	97.4 %	98.2 %	97.5 %
Repr[b] PEG	97.9 %	99.2 %	98.3 %	98.6 %	98.4 %	95.2 %	98.8 %	96.7 %	98.8 %
Repr[b] DMSO	99.6 %	94.2 %	96.3 %	97.9 %	92.6 %	95.9 %	98.6 %	98.0 %	97.7 %
SNR[c] H_2O	77	114	103	258	250	291	136	140	135

[a] ADCs (and their errors) in units of 10^{-3} mm^2/s averaged over all 4 repetitions of measurements;
[b] Reproducibility (1 – standard deviation / mean value) with respect to the 4 repetitions;
[c] Signal-to-noise ratio in H_2O with b-value of 50 s/mm^2.

Table 3. Comparison of diffusion measurements in excised tumor tissue and muscle.

Sample	Tissue	SE Read	SE Phase	SE Slice	mRARE Read	mRARE Phase	mRARE Slice	EPI Read
1	muscle	0.910 (0.015)	0.874 (0.012)	1.186 (0.010)	0.908 (0.020)	1.022 (0.028)	1.166 (0.018)	0.915 (0.007)
	liposarcoma, grade 1	0.087 (0.001)	0.066 (0.004)	0.088 (0.004)	0.204 (0.012)	0.244 (0.153)	0.382 (0.007)	0.381 (0.028)
2	muscle	0.931 (0.004)	0.892 (0.008)	1.206 (0.023)	0.925 (0.014)	0.999 (0.021)	1.196 (0.014)	0.936 (0.003)
	high-grade pleomorphic sarcoma	0.647 (0.004)	0.550 (0.011)	0.564 (0.018)	0.698 (0.012)	0.698 (0.004)	0.631 (0.017)	0.617 (0.009)
3	muscle	0.948 (0.015)	0.982 (0.012)	1.223 (0.010)	1.068 (0.020)	1.126 (0.011)	1.259 (0.021)	1.045 (0.009)
	liposarcoma, grade 3	0.494 (0.021)	0.519 (0.015)	0.539 (0.011)	0.591 (0.019)	0.632 (0.008)	0.598 (0.017)	0.554 (0.012)
4	muscle	1.039 (0.010)	1.015 (0.009)	1.205 (0.008)	1.076 (0.021)	1.159 (0.015)	1.226 (0.025)	1.074 (0.013)
	carcinosarcoma	0.601 (0.014)	0.586 (0.014)	0.621 (0.008)	0.677 (0.020)	0.718 (0.015)	0.703 (0.020)	0.648 (0.010)

ADCs (and their errors) in units of 10^{-3} mm^2/s.

Measurements of excised tumor tissue and muscle

ADCs determined in excised and fixated tumor tissue and in muscle tissue are summarized in Table 3. The deviation of the ADC in muscle measured by the mRARE sequence from the average ADC of the SE and EPI sequence (all in readout direction) was 0.5 % in sample 1, 0.8 % in sample 2, 7.2 % in sample 3, and 1.9 % in sample 4. The corresponding values in the tumor tissue were 12.8 %, 10.5 %, 12.8 %, and 8.4 %, respectively. The estimated diffusion anisotropy in muscle tissue measured by the SE sequence was 1.36 (standard deviation 0.03), 1.35 (0.04), 1.29 (0.05), and 1.19 (0.02) for the 4 samples. The estimated diffusion anisotropy in tumor tissue was 1.33 (0.14), 1.18 (0.03), 1.09 (0.07), and 1.06 (0.04), respectively. For the mRARE sequence, the estimated anisotropy in the 4 samples was 1.28 (0.05), 1.29 (0.03), 1.18 (0.04), and 1.14 (0.05) in muscle tissue and 1.87 (0.15), 1.11 (0.05), 1.07 (0.05), and 1.06 (0.05) in tumor tissue.

Image examples of the diffusion measurements and the resulting ADC maps are shown in Fig. 2. In contrast to the SE and mRARE images, the EPI images show gross geometric distortions. Blurring affects the EPI and especially the mRARE images, resulting in an effectively lower spatial resolution than in the SE image. In general, image quality of these measurements was very similar to the phantom measurements described above; however, no motion artifacts were visible in the SE images. While ROIs could be copied from SE to mRARE images, different ROIs had to be used for the echo-planar images because of the geometric distortions.

Patient measurements

A summary of results of the diffusion measurements in patients is given in Table 4. In all examined patients, the quality of the diffusion-weighted images was sufficient to determine the ADC in the tumor. The ADC ratio in tumor tissue of measurements using the EPI and the mRARE sequence ranged from 0.617 to 1.247 with a mean value of 1.06 and a standard deviation of 0.17. The Wilcoxon matched-pairs signed-ranks test showed no significant difference between the ADCs of tumor tissue (solid and cystic) and muscle edema measured by the mRARE on the one hand and the EPI sequence on the other hand (number of measurements $n = 12$, $p = 0.12$). In non-edematous muscle, the ADC ratio varied between 0.443 and 3.030 with a mean value 1.42 and a standard deviation of 1.40.

Figures 3–6 show image examples of diffusion-weighted images and ADC maps from different anatomic regions. In all cases, the mRARE sequence provided better anatomic orientation because, in contrast to the EPI sequence, images could be acquired without fat suppression and more tissue out-

side the tumor itself is visible. The echo-planar images in Fig. 5 are affected by imperfect fat suppression and signal from subcutaneous fat shifted in anterior direction; the corresponding ADC map shows a lateral signal void that does not appear in the ADC map calculated from the mRARE images. In Fig. 6 considerable N/2-ghosting can be observed in the EPI data.

Table 4. Diffusion coefficients in musculoskeletal soft-tissue tumors in vivo.

Patient	Tumor	Localization	Tissue	ADC[1] mRARE	ADC[1] EPI	Ratio mRARE /EPI
1: 74 y, m	osteosarcoma	upper arm	tumor	1.263 (0.053)	1.206 (0.066)	1.047
2: 63 y, m	liposarcoma, grade 3	thigh	solid tumor	1.248 (0.056)	1.069 (0.033)	1.167
			cystic tumor	2.728 (0.039)	2.435 (0.027)	1.120
			muscle	0.768 (0.050)	0.968 (0.135)	0.793
3: 60 y, f	high-grade sarcoma	thigh	solid tumor	1.427 (0.097)	1.144 (0.076)	1.247
			muscle	0.603 (0.052)	0.199 (0.097)	3.030
4: 61 y, m	myxoid liposarcoma, grade 1	proximal femur	cystic tumor	2.591 (0.227)	2.302 (0.096)	1.126
			muscle	0.478 (0.044)	(*)	–
5: 68 y, f	MFH (malignant fibrous histiocytoma)	knee	solid tumor	1.338 (0.055)	1.127 (0.038)	1.187
			cystic tumor	2.719 (0.053)	2.622 (0.078)	1.037
6: 78 y, m	MFH	thigh	solid tumor	1.307 (0.180)	1.089 (0.044)	1.200
			muscle edema	1.813 (0.338)	2.008 (0.046)	0.903
			muscle	0.447 (0.055)	1.008 (*)	0.443
7: 48 y, m	spindle cell sarcoma	foot	solid tumor	1.159 (0.081)	1.079 (0.046)	1.074
8: 71 y, m	high-grade sarcoma	pelvis	solid tumor	0.924 (0.034)	0.956 (0.075)	0.967
9: 68 y, f	liposarcoma, grade 1	thigh	solid tumor	0.841 (0.231)	1.364 (*)	0.617
			muscle	0.577 (0.111)	(*)	–

ADCs (and their errors) in units of 10^{-3} mm^2/s.
(*) could not be determined because SNR was too low

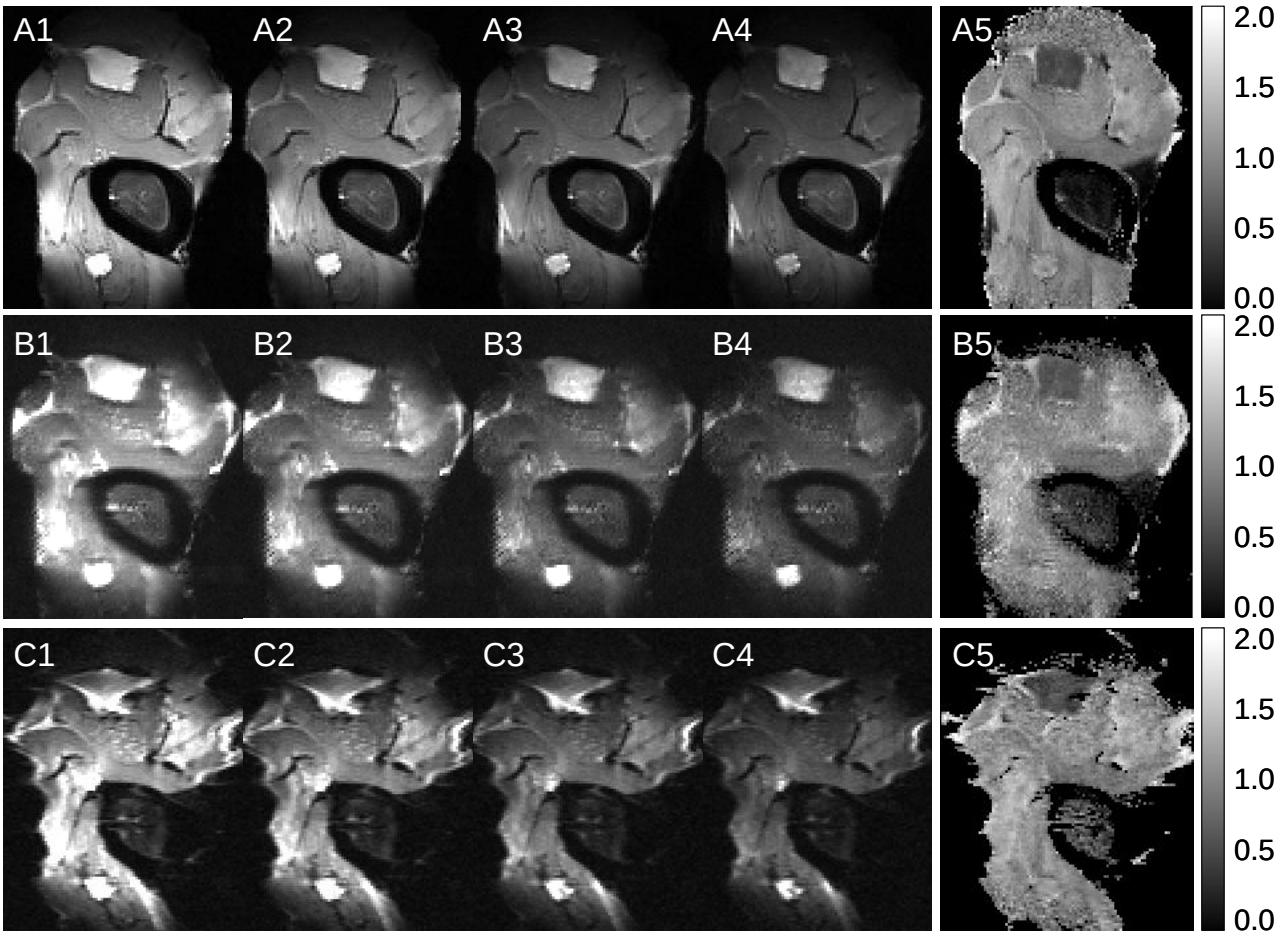

Figure 2: Image examples of diffusion measurements in excised tumor tissue embedded in bovine muscle. Row A: spin echo sequence, row B: single-shot multiple spin-echo sequence, row C: EPI sequence. Column 1…4: diffusion-weighted images with b-values 50, 250, 500, and 750 s/mm^2, column 5: ADC maps, scaled from 0 to 2.0×10^{-3} mm^2/s.

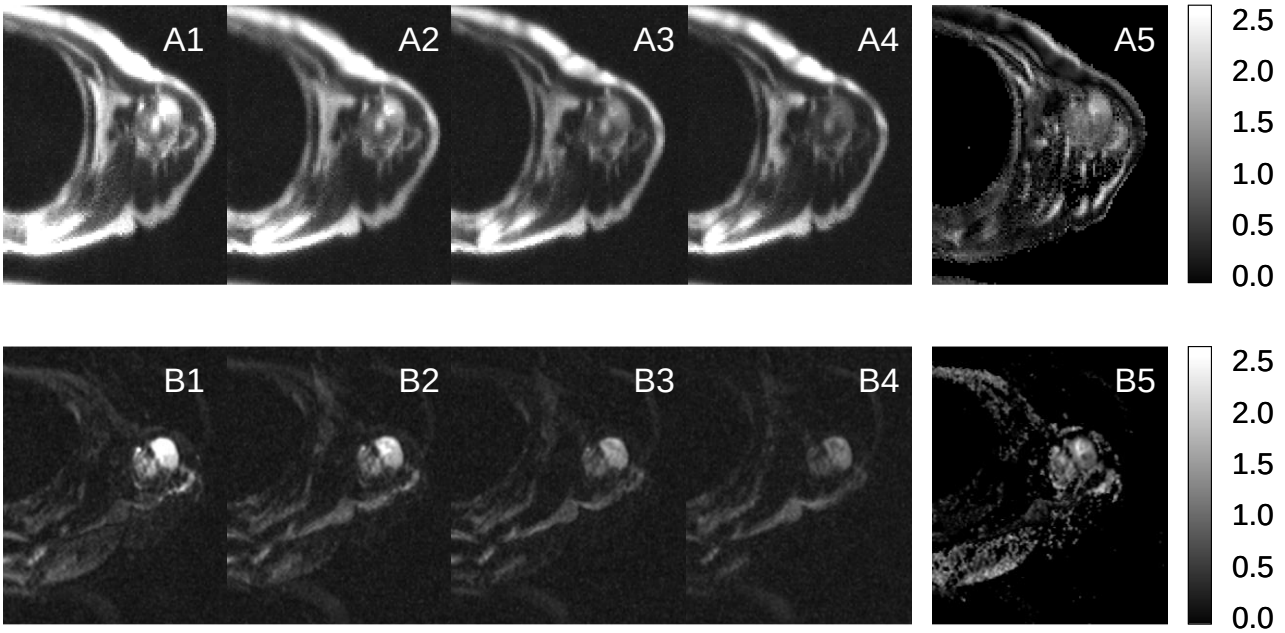

Figure 3: Diffusion-weighted images of patient 1 suffering from an osteosarcoma in his left humerus. Row A: single-shot multiple spin-echo sequence, row B: EPI sequence. Column 1…4: diffusion-weighted images with b-values 50, 250, 500, and 750 s/mm^2, column 5: ADC maps, scaled from 0 to 2.5×10^{-3} mm^2/s.

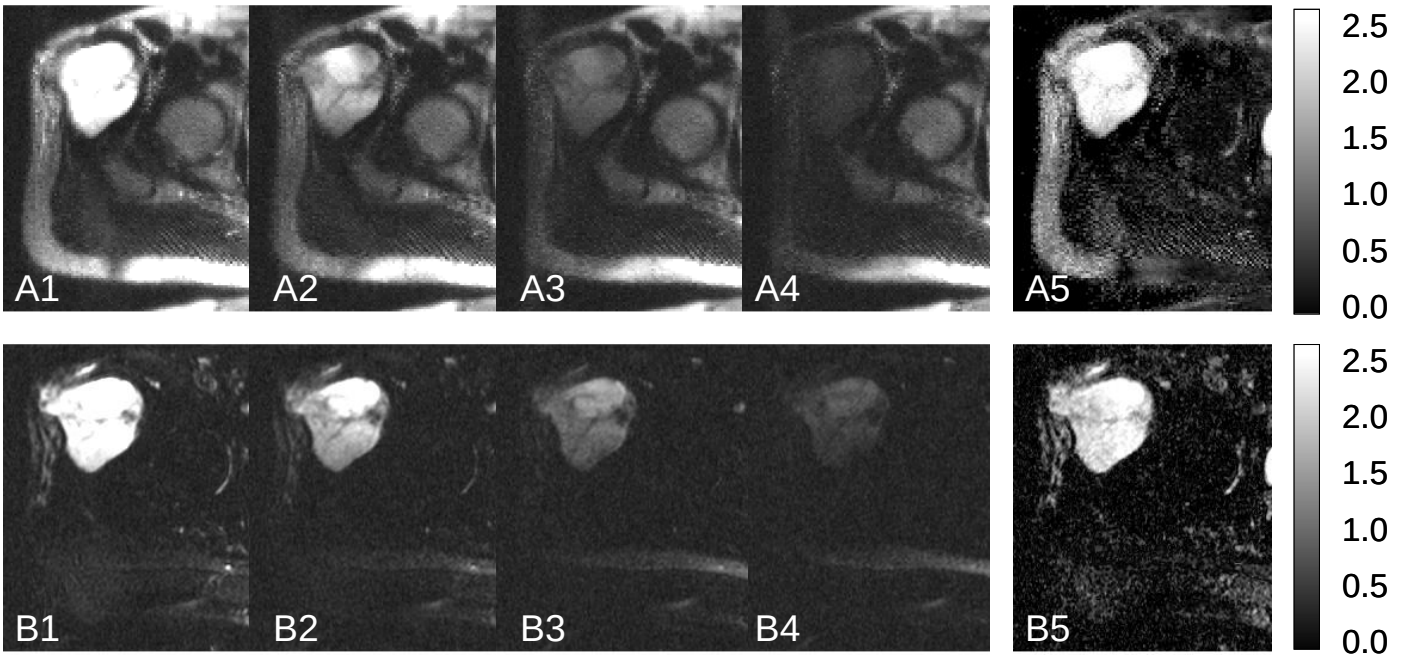

Figure 4: Diffusion-weighted images of patient 4 suffering from a myxoid liposarcoma at the lateral side of the proximal femur. Row A: single-shot multiple spin-echo sequence, row B: EPI sequence. Column 1…4: diffusion-weighted images with b-values 50, 250, 500, and 750 s/mm^2, column 5: ADC maps, scaled from 0 to 2.5×10^{-3} mm^2/s.

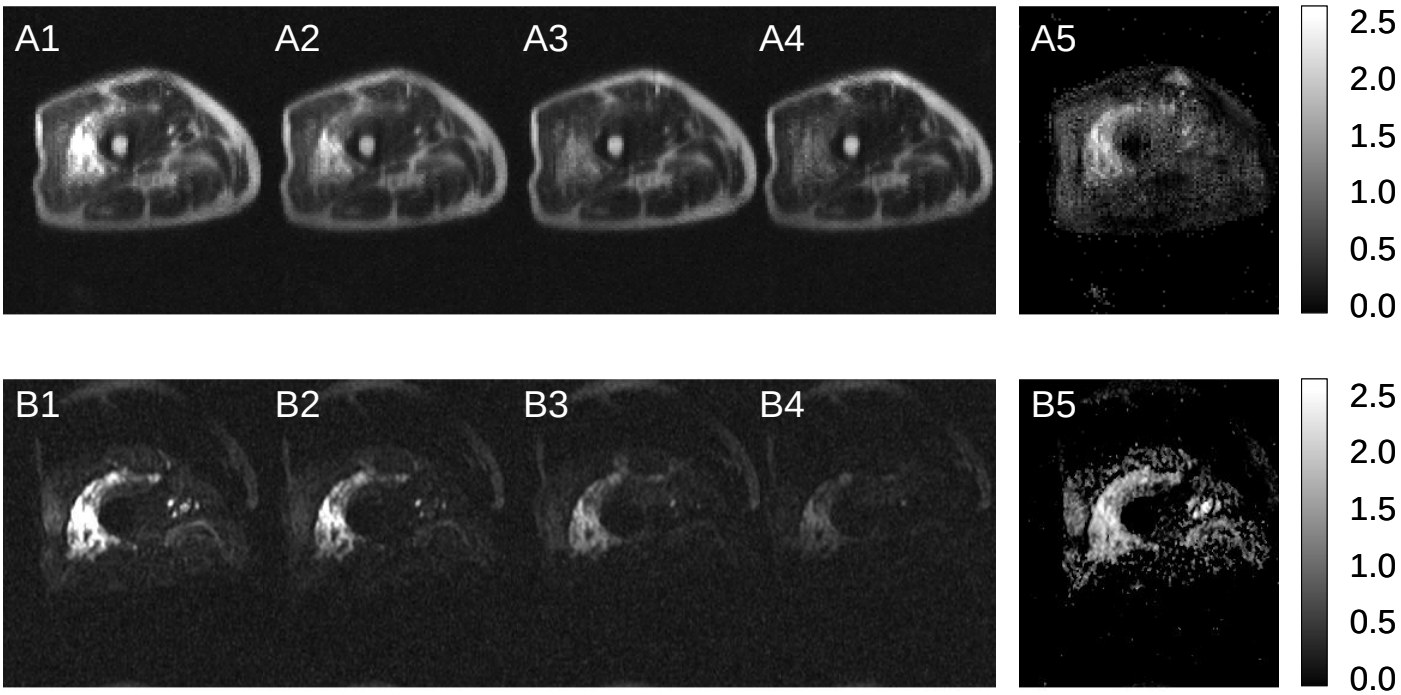

Figure 5: Diffusion-weighted images of patient 6 suffering from a pleomorphic sarcoma in his right thigh; the images show muscle edema adjacent to the tumor. Row A: single-shot multiple spin-echo sequence, row B: EPI sequence. Column 1…4: diffusion-weighted images with b-values 50, 250, 500, and 750 s/mm^2, column 5: ADC maps, scaled from 0 to 2.5×10^{-3} mm^2/s.

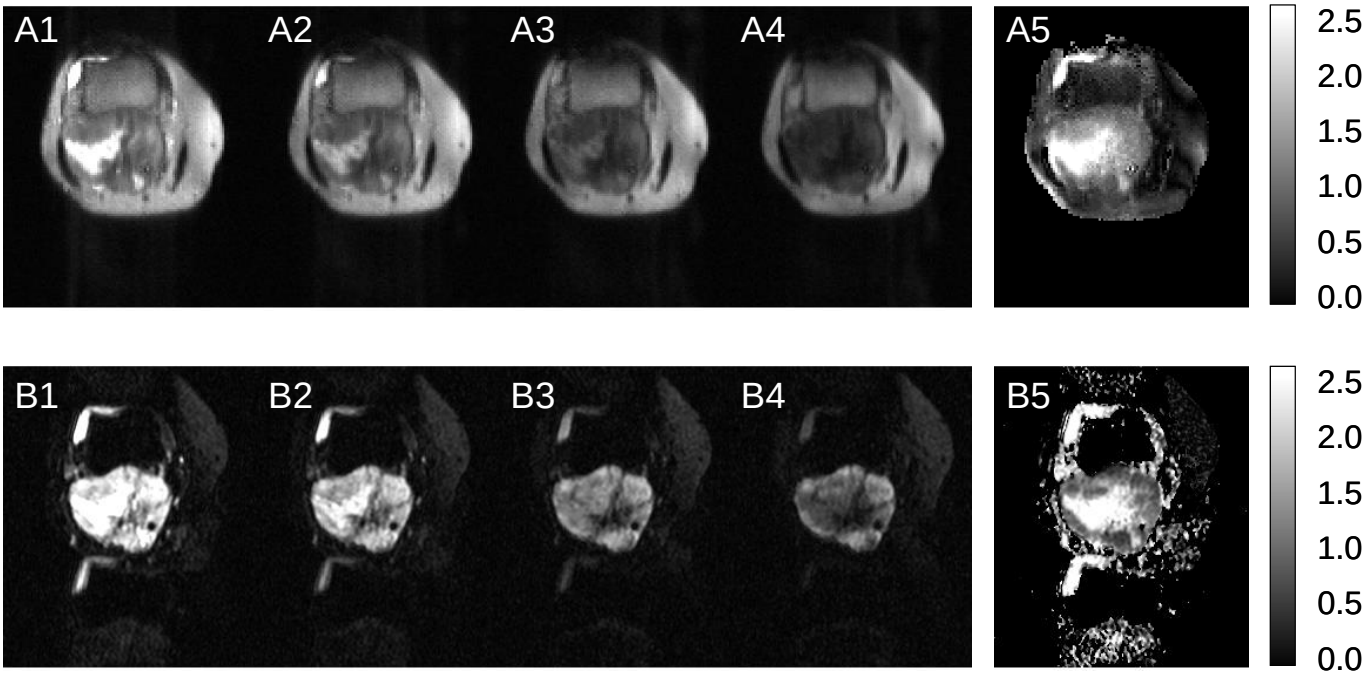

Figure 6: Diffusion-weighted images of patient 5 suffering from a pleomorphic high-grade sarcoma in the dorsal compartment of his knee. Row A: single-shot multiple spin-echo sequence, row B: EPI sequence. Column 1…4: diffusion-weighted images with b-values 50, 250, 500, and 750 s/mm^2, column 5: ADC maps, scaled from 0 to 2.5×10^{-3} mm^2/s.

Discussion

In this study we evaluated the feasibility of a diffusion-weighting single-shot mRARE sequence for DWI of soft-tissue tumors in the musculoskeletal system by imaging experiments in phantoms, in vitro, and in vivo. The results of these experiments were compared with data acquired by a conventional spin echo sequence and a single-shot EPI sequence.

The diffusion coefficients of the phantom measurements showed very good agreement for all sequence types in water and DMSO. However, we observed considerable variations in measurements in acetone that can be explained by the low base signal in acetone (cf. Fig. 1) and the very high motion sensitivity due to its high diffusivity. Taking into account the homogeneity of the diffusion coefficient in the different diffusion directions and the magnitude of the error of the linear regression, the EPI sequence probably gave the best results for acetone with approximately 3.5×10^{-3} mm^2/s. The diffusivity determined in PEG agrees well in the mRARE and EPI experiment but differs in the SE measurement. This result might be related to the occurrence of two resonance lines in PEG that are visualized as double contours in the echo-planar images (cf. Fig. 1); in-phase/opposed-phase effects due to different echo times in the three different pulse sequences may have influenced the diffusion measurements.

Excluding the acetone phantom, we found a very high reproducibility of more than 95 % for the diffusion measurements with all three sequence types. Based on these quantitative results alone, all three pulse sequences appear equally suited for diffusion measurements in regions of interests within liquid phantoms; however, image quality was very different for the three techniques. Particularly the EPI sequence showed gross geometric distortions and N/2-ghosting in phase-encoding (left–right) direction. Image quality of the SE sequence varied with the diffusion weighting and the diffusion direction: e.g., at high b-values and diffusion-gradients in phase-encoding direction, motion artifacts appeared probably related to motion of the scanner table due to the gradient switching. Although some image artifacts are visible in the DMSO phantom when using the mRARE sequence, this technique probably provides the best compromise between image quality and stability of the results.

The measurements of the ADC in excised tumor tissue and bovine muscle was performed to compare the examined diffusion sequences under mechanical, susceptibility, relaxation, and diffusion conditions similar to human tissue in vivo. Although the molecular structure of biologic tissue changes within

minutes after the blood supply ceases, these in vitro experiments are considerably closer to measurements in vivo than phantom experiments with test liquids. The range of relaxation times (T1/T2) and, in particular, the susceptibility effects and mechanical reaction to scanner motion of biological tissue are hardly reproducible with liquid phantoms. Liquids are very sensitive to motion induced by gradient switching and thus, fluctuations can occur that influence diffusion measurements. Local variations of susceptibility are caused by transitions between soft tissue and bone or between tissue and air and induce characteristic geometric distortions. In order to evaluate these effects, experiments in biologic tissue are required, but in vivo experiments are not suitable to compare different sequences in repeated measurements under identical conditions. Therefore, DWI in excised tumor tissue and bovine muscle was chosen as intermediate step between phantom measurements and clinical in vivo application.

The measurements in excised tumor tissue showed also good agreement of the mRARE approach with the SE and EPI methods. Especially in muscle, the different techniques agreed within a range of 0.5 % to 7 %. The calculated ADCs of muscle are compatible with an earlier ex vivo study that presented mean diffusion coefficients of 0.9×10^{-3} mm^2/s in bovine muscle [36]. In tumor tissue, the difference between the methods was about 10 %, which is reasonable regarding the comparably low ADCs between 0.1 and 0.7×10^{-3} mm^2/s. For such low ADCs, the b-value range should ideally be extended up to at least 2000 s/mm^2; however, this would require much longer echo times and thus reduce the SNR. Therefore, a certain loss in accuracy must be accepted when measuring low ADCs.

Determination of the ADC in three orthogonal directions enabled us to estimate the diffusion anisotropy of the examined tissue. Since the determination of anisotropy is very sensitive to noise and statistical errors [37], the results in tumor tissue must be regarded with special care, particularly in the first sample with its low diffusivity. In cases of low ADCs and a limited b-value range, the determination of the diffusion coefficient suffers from considerable statistical errors that propagate to the calculated anisotropy. Whereas the data quality in tumor tissue is therefore not sufficient to confirm or disprove anisotropic diffusion, the anisotropy in muscle could be determined with lower standard deviations and is in good agreement with published data that describes an increased diffusivity parallel to the muscle fiber direction (slice direction in our experiments) and ADC ratios of maximum and minimum diffusion coefficient between 1.2 and 1.4 [15].

The ADC measurements of tumor tissue in patients showed an acceptable agreement of the mRARE and EPI technique with typical differences of less than 15 % that were statistically not significant ($p = 0.12$). In cystic areas of the tumors we consistently determined ADCs greater than 2.0×10^{-3} mm^2/s. In solid tumor tissue we found ADCs between 0.8 and 1.4×10^{-3} mm^2/s. These values are in the same range as reported by Wang et al. [20] for malignant lesions in the head and neck, which, however, were of different types (adenocarcinoma, squamous cell carcinoma) than the tumors in the present study. Results published by van Rijswisk et al. [21] are difficult to compare to our data because of the different tumor (sub)types and the large variations of ADCs reported. A comparison is possible for the myxoid liposarcoma in patient 4 in whom our results, 2.59 ± 0.23 (mRARE) and $2.30\pm0.10\times10^{-3}$ mm^2/s (EPI), agree well with the ADC of 2.20×10^{-3} mm^2/s given by van Rijswijk. A recent study of Einarsdóttir et al. [22] reports ADCs in sarcomas between 0.9 and 2.3×10^{-3} mm^2/s (the latter again in a myxoid liposarcoma) and thus shows general agreement with our data.

The ADCs that we determined in skeletal muscle are about 50 % to 70 % lower than values presented in literature [15, 16]. An explanation might be that earlier studies examined young healthy volunteers whereas our measurements were performed in older patients suffering from musculoskeletal tumors, and the evaluated regions were positioned relatively close to the tumor. To our knowledge neither the age dependence nor the influence of muscle atrophy, neighboring lesions, or edema on the ADC of skeletal muscle has yet been investigated.

The choice of b-values used in this study is a compromise between sufficiently high diffusion weighting and acceptable echo times. Because of the short T2 relaxation times of many musculoskeletal structures, a shorter TE compared to DWI of the brain is desirable although this limits the maximum possible b-value. Our maximum b-value of 750 s/mm^2 was in the same range as in comparable earlier studies that used diffusion weightings up to 701 s/mm^2 [21], 1000 s/mm^2 [20], or 600 s/mm^2 [22]. To avoid the influence of perfusion effects we used a minimum b-value of 50 s/mm^2, thus achieving a similar effect as van Rijswijk et al. by calculating the "true diffusion coefficient" [21]. Spending the time for the acquisition of 4 different diffusion weightings

(50, 250, 500, and 750 s/mm^2) instead of increasing the number of averages of the highest b-value slightly reduces the accuracy of the ADC determination [38], but has the advantage that the measurement error can be estimated by comparing the signal attenuation to the expected mono-exponential decay.

The sequence parameters of the compared sequences, in particular TE, TR, bandwidth, and number of averages differ considerably. The choice of parameters was required by the different sequence techniques; e.g., the TR of the SE sequence had to be chosen shorter to reduce the total measurement time, and the bandwidth of the EPI sequence had to be increased to reduce susceptibility artifacts and T2* decay during the echo train. The TE of the mRARE sequence could not be further reduced due to the desired b-value of 750 s/mm² and the required dummy scans; in order to compensate for the long TE and the lower SNR the number of averages had to be increased. However, these parameters do not influence directly the ADC determination that depends only on the signal differences of images acquired with varying b-values but with identical imaging parameters as was demonstrated in our phantom measurements.

The three studies referenced above use single-shot EPI [20], multi-shot EPI [22], and conventional pulse-triggered SE [21] pulse sequences. Historically, the diffusion-weighting SE sequence was one of the first used for DWI measurements in vivo [39]. However, diffusion-weighting SE sequences suffer from long acquisition times and are very sensitive to motion artifacts even in liquid phantoms as we observed in this study and even more so in vivo. Therefore, today the most commonly used sequences for DWI are diffusion-weighting spin-echo single-shot EPI sequences, which are especially useful for DWI and DTI of the brain. Advantages of the EPI approach are very fast imaging (about 100 ms per slice) and low motion sensitivity. Unfortunately, EPI sequences are very sensitive to chemical shift and susceptibility artifacts and thus require a very homogeneous B_0 field, good fat saturation, and little local field variations that typically occur at transitions e.g. between soft tissue and bone or between tissue and air. Therefore, EPI sequences are much better suited for DWI of the brain than for DWI of musculoskeletal structures which typically show larger variations in susceptibility and less efficient fat suppression. Because of the increased technical difficulty and the occurrence of gross image artifacts, considerably fewer studies about DWI outside the brain have been published than about DWI of the brain.

Multi-shot EPI sequences are a compromise between the EPI and the SE approach. On the one hand they are less sensitive to susceptibility variations than single-shot EPI, but on the other hand they require longer acquisition times and are much more sensitive to motion and therefore, they are usually combined with navigator motion correction, i.e., an additional step in post-processing that reduces the robustness of these sequence type.

The single-shot mRARE approach analyzed in this article combines the advantages of single-shot imaging (short acquisition time, low motion sensitivity) with the good geometric image quality (absence of distortions) of conventional SE and TSE sequences as we demonstrated in phantom measurements. However, due to both the longer duration of the echo train compared to single-shot EPI and additional signal loss because of imperfect refocusing RF pulses, mRARE images are affected by increased blurring. A second disadvantage is the relative low SNR caused by the repeated application of refocusing RF pulses (required for diffusion preparation and dummy readouts) before the central k-space line is acquired, and by the suppression of all echoes of odd parity [33]. To overcome the low SNR, we repeated the measurements 10 times and averaged the resulting magnitude images; this approach increased the SNR above the level of the SE and EPI sequence used in this study. Future improvements of the mRARE approach should include the application of parallel imaging [40, 41] to reduce the echo train length and, thereby, blurring of the sequence. Depending on the transversal relaxation times, single-shot parallel imaging might affect the SNR as well; in this case a part of the time gained by imaging acceleration might be spent to acquire an increased number of averages.

Other techniques like Line Scan Imaging [42] or PROPELLER imaging [43] have been suggested for robust DWI; however, these methods have not yet been evaluated for diffusion measurements of musculoskeletal tumors. A disadvantage of these newer techniques is their very limited availability since they have not yet been added to the set of product pulse sequences by most manufacturers. SSFP pulse sequences as a further alternative technique have the disadvantage that the ADC cannot be easily determined.

In conclusion, we have demonstrated that the described diffusion-weighting multiple spin echo pulse sequence, a variant of a centric-reordered RARE sequence, is feasible for the acquisition of diffusion-

weighted images of musculoskeletal soft-tissue tumors and for the quantification of the apparent diffusion coefficient in tumors. Diffusion-weighted images were less distorted than those acquired with a single-shot EPI sequence and provided more anatomic information since muscle and fat signals were considerably higher. ADCs determined with both methods agreed well. These properties recommend the mRARE diffusion sequence for further studies in larger patient groups with musculoskeletal tumors aimed e.g. on differentiation of benign and malignant lesions or of tumor recurrences and post-therapeutic soft-tissue changes.

Acknowledgement

This work was supported by the Deutsche Forschungsgemeinschaft (DFG), Grant Nos. BA 2089/1-1 and BA 2089/1-3.

References

1. Moseley ME, Cohen Y, Mintorovitch J, Chileuitt L, Shimizu H, Kucharczyk J, Wendland MF, Weinstein PR (1990) Early detection of regional cerebral ischemia in cats: comparison of diffusion- and T2-weighted MRI and spectroscopy. Magn Reson Med 14:330–346.
2. Chien D, Kwong KK, Gress DR, Buonanno FS, Buxton RB, Rosen BR (1992) MR diffusion imaging of cerebral infarction in humans. AJNR Am J Neuroradiol 13:1097–1102.
3. Huisman TA (2003) Diffusion-weighted imaging: basic concepts and application in cerebral stroke and head trauma. Eur Radiol 13:2283–2297. DOI 10.1007/s00330-003-1843-6
4. Douek P, Turner R, Pekar J, Patronas N, Le Bihan D (1991) MR color mapping of myelin fiber orientation. J Comput Assist Tomogr 15:923–929.
5. Pierpaoli C, Jezzard P, Basser PJ, Barnett A, Di Chiro G (1996) Diffusion tensor MR imaging of the human brain. Radiology 201:637–648.
6. Jones DK, Williams SC, Gasston D, Horsfield MA, Simmons A, Howard R (2002) Isotropic resolution diffusion tensor imaging with whole brain acquisition in a clinically acceptable time. Hum Brain Mapp 15:216–230. DOI 10.1002/hbm.10018
7. Tievsky AL, Ptak T, Farkas J (1999) Investigation of apparent diffusion coefficient and diffusion tensor anisotrophy in acute and chronic multiple sclerosis lesions. AJNR Am J Neuroradiol 20:1491–1499.
8. Werring DJ, Clark CA, Barker GJ, Thompson AJ, Miller DH (1999) Diffusion tensor imaging of lesions and normal-appearing white matter in multiple sclerosis. Neurology 52:1626–1632.
9. Kim YJ, Chang KH, Song IC, Kim HD, Seong SO, Kim YH, Han MH (1998) Brain abscess and necrotic or cystic brain tumor: discrimination with signal intensity on diffusion-weighted MR imaging. AJR Am J Roentgenol 171:1487–1490.
10. Sugahara T, Korogi Y, Kochi M, Ikushima I, Shigematu Y, Hirai T, Okuda T, Liang L, Ge Y, Komohara Y, Ushio Y, Takahashi M (1999) Usefulness of diffusion-weighted MRI with echo-planar technique in the evaluation of cellularity in gliomas. J Magn Reson Imaging 9:53–60. DOI 10.1002/(SICI)1522-2586(199901)9:1<53::AID-JMRI7>3.0.CO;2-2
11. Taouli B, Vilgrain V, Dumont E, Daire JL, Fan B, Menu Y (2003) Evaluation of liver diffusion isotropy and characterization of focal hepatic lesions with two single-shot echo-planar MR imaging sequences: prospective study in 66 patients. Radiology 226:71–78. DOI 10.1148/radiol.2261011904
12. Ries M, Jones RA, Basseau F, Moonen CT, Grenier N (2001) Diffusion tensor MRI of the human kidney. J Magn Reson Imaging 14:42–49. DOI 10.1002/jmri.1149
13. Cova M, Squillaci E, Stacul F, Manenti G, Gava S, Simonetti G, Pozzi-Mucelli R (2004) Diffusion-weighted MRI in the evaluation of renal lesions: preliminary results. Br J Radiol 77:851–857. DOI 10.1259/bjr/26525081
14. Moteki T, Ishizaka H (1999) Evaluation of cystic ovarian lesions using apparent diffusion coefficient calculated from reordered turboflash MR images. Magn Reson Imaging 17:955–963. DOI 10.1016/S0730-725X(99)00036-3
15. Sinha U, Yao L (2002) In vivo diffusion tensor imaging of human calf muscle. J Magn Reson Imaging 15:87–95. DOI 10.1002/jmri.10035
16. Nygren AT, Kaijser L (2002) Water exchange induced by unilateral exercise in active and inactive skeletal muscles. J Appl Physiol 93:1716–1722. DOI 10.1152/japplphysiol.01117.2001
17. Eustace S, DiMasi M, Adams J, Ward R, Caruthers S, McAlindon T (2000) In vitro and in vivo spin echo diffusion imaging characteristics of synovial fluid: potential non-invasive differentiation of inflammatory and degenerative arthritis. Skeletal Radiol 29:320–323. DOI 10.1007/s002560000204
18. Dietrich O, Herlihy A, Dannels WR, Fiebach J, Heiland S, Hajnal JV, Sartor K (2001) Diffusion-weighted imaging of the spine using radial k-space trajectories. MAGMA 12:23–31. DOI 10.1016/S1352-8661(00)00132-0
19. Baur A, Huber A, Arbogast S, Durr HR, Zysk S, Wendtner C, Deimling M, Reiser M (2001) Diffusion-weighted imaging of tumor recurrencies and posttherapeutical soft-tissue changes in humans. Eur Radiol 11:828–833. DOI 10.1007/s003300000761
20. Wang J, Takashima S, Takayama F, Kawakami S, Saito A, Matsushita T, Momose M, Ishiyama T (2001) Head and neck lesions: characterization with diffusion-weighted echo-planar MR imaging. Radiology 220:621–630. DOI 10.1148/radiol.2202010063
21. van Rijswijk CS, Kunz P, Hogendoorn PC, Taminiau AH, Doornbos J, Bloem JL (2002) Diffusion-weighted MRI in the characterization of soft-tissue tumors. J Magn Reson

Imaging 15:302–307.
DOI 10.1002/jmri.10061

22. Einarsdóttir H, Karlsson M, Wejde J, Bauer HC (2004) Diffusion-weighted MRI of soft tissue tumours. Eur Radiol 14:959–963.
DOI 10.1007/s00330-004-2237-0
23. Baur A, Stabler A, Bruning R, Bartl R, Krodel A, Reiser M, Deimling M (1998) Diffusion-weighted MR imaging of bone marrow: differentiation of benign versus pathologic compression fractures. Radiology 207:349–356.
24. Nonomura Y, Yasumoto M, Yoshimura R, Haraguchi K, Ito S, Akashi T, Ohashi I (2001) Relationship between bone marrow cellularity and apparent diffusion coefficient. J Magn Reson Imaging 13:757–760.
DOI 10.1002/jmri.1105
25. Zhou XJ, Leeds NE, McKinnon GC, Kumar AJ (2002) Characterization of benign and metastatic vertebral compression fractures with quantitative diffusion MR imaging. AJNR Am J Neuroradiol 23:165–170.
26. Park SW, Lee JH, Ehara S, Park YB, Sung SO, Choi JA, Joo YE (2004) Single shot fast spin echo diffusion-weighted MR imaging of the spine; Is it useful in differentiating malignant metastatic tumor infiltration from benign fracture edema? Clin Imaging 28:102–108.
DOI 10.1016/S0899-7071(03)00247-X
27. Bammer R, Herneth AM, Maier SE, Butts K, Prokesch RW, Do HM, Atlas SW, Moseley ME (2003) Line scan diffusion imaging of the spine. AJNR Am J Neuroradiol 24:5–12.
28. Baur A, Dietrich O, Reiser M (2003) Diffusion-weighted imaging of bone marrow: current status. Eur Radiol 13:1699–1708.
DOI 10.1007/s00330-003-1873-0
29. Lang P, Wendland MF, Saeed M, Gindele A, Rosenau W, Mathur A, Gooding CA, Genant HK (1998) Osteogenic sarcoma: noninvasive in vivo assessment of tumor necrosis with diffusion-weighted MR imaging. Radiology 206:227–235.
30. Stejskal EO, Tanner JE (1965) Spin diffusion measurements: Spin echoes in the presence of a time-dependent field gradient. J Chem Phys 42:288–292.
31. Hennig J, Nauerth A, Friedburg H (1986) RARE imaging: a fast imaging method for clinical MR. Magn Reson Med 3:823–833.
32. Norris DG (1991) Ultrafast low-angle RARE: U-FLARE. Magn Reson Med 17:539–542.
33. Norris DG, Bornert P, Reese T, Leibfritz D (1992) On the application of ultra-fast RARE experiments. Magn Reson Med 27:142–164.
34. Reese TG, Heid O, Weisskoff RM, Wedeen VJ (2003) Reduction of eddy-current-induced distortion in diffusion MRI using a twice-refocused spin echo. Magn Reson Med 49:177–182.
DOI 10.1002/mrm.10308
35. Firbank MJ, Coulthard A, Harrison RM, Williams ED (1999) A comparison of two methods for measuring the signal to noise ratio on MR images. Phys Med Biol 44:N261–N264
DOI 10.1088/0031-9155/44/12/403
36. Bonny JM, Renou JP (2002) Water diffusion features as indicators of muscle structure ex vivo. Magn Reson Imaging 20:395400.
DOI 10.1016/S0730-725X(02)00515-5
37. Bastin ME, Armitage PA, Marshall I (1998) A theoretical study of the effect of experimental noise on the measurement of anisotropy in diffusion imaging. Magn Reson Imaging 16:773–785.
DOI 10.1016/S0730-725X(98)00098-8
38. Jones DK, Horsfield MA, Simmons A (1999) Optimal strategies for measuring diffusion in anisotropic systems by magnetic resonance imaging. Magn Reson Med 42:515–525.
DOI 10.1002/(SICI)1522-2594(199909)42:3<515::AID-MRM14>3.0.CO;2-Q
39. Le Bihan D, Breton E, Lallemand D, Grenier P, Cabanis E, Laval-Jeantet M (1986) MR imaging of intravoxel incoherent motions: application to diffusion and perfusion in neurologic disorders. Radiology 161:401–407.
40. Dietrich O, Nikolaou K, Wintersperger BJ, Flatz W, Nittka M, Petsch R, Kiefer B, Schoenberg SO (2002) iPAT: Applications for fast and cardiovascular MR imaging. Electromedica 70:133–146.
41. Heidemann RM, Ozsarlak O, Parizel PM, Michiels J, Kiefer B, Jellus V, Muller M, Breuer F, Blaimer M, Griswold MA, Jakob PM (2003) A brief review of parallel magnetic resonance imaging. Eur Radiol 13:2323–2337.
DOI 10.1007/s00330-003-1992-7
42. Gudbjartsson H, Maier SE, Mulkern RV, Morocz IA, Patz S, Jolesz FA (1996) Line scan diffusion imaging. Magn Reson Med 36:509–519.
43. Pipe JG, Farthing VG, Forbes KP (2002) Multishot diffusion-weighted FSE using PROPELLER MRI. Magn Reson Med 47:42–52.
DOI 10.1002/mrm.10014